Available online at www.sciencedirect.com
SCIENCE DIRECT®
C. R. Chimie 8 (2005) 353–368
COMPTES RENDUS CHIMIE
http://france.elsevier.com/direct/CRAS2C/

Full paper / Mémoire

Structural investigations on zeolitic faujasite/benzene host/guest systems (Si/Al = 2.43 and ≈ 200) by using combined powder diffraction, adsorption calorimetry and molecular mechanics simulations

Bernard F. Mentzen *

5, rue Marcel-Desplaces, 69330 Meyzieu, France

Received 12 April 2004; accepted after revision 15 November 2004

Available online 26 February 2005

Abstract

The NaY(Si/Al =2.43)/benzene (1) and DAY(Si/Al ≈ 200)/benzene (2) systems are investigated by combined adsorption calorimetry, X-ray or neutron powder diffraction and computer simulation techniques. For (1) and (2) a good estimation of the sorption heats is obtained. A complementary study of a prehydrated NaY/benzene (3) system is also realized. For (1), (2) and (3) the BZ(C)/BZ(W) ratios, the distributions (localization and population) of these two independent sorbate species and the variations of the cubic unit-cell parameters are given. In (3) two ordered WI′ and WII water species exist and their distributions are reported. For this system a substantial cation migration is evidenced. In (2) two independent and totally disordered benzene species exist. It is concluded that adsorption calorimetry yields decisive informations on the adsorption mechanisms. ***To cite this article: B.F. Mentzen, C. R. Chimie 8 (2005).***

Résumé

Une étude comparée des systèmes NaY(Si/Al = 2,43)/benzène (1) et DAY(Si/Al ≈ 200)/benzène (2) par calorimétrie d'adsorption, diffraction X ou neutronique sur poudres et calculs théoriques est effectuée. Pour (1) et (2), une bonne estimation des énergies d'adsorption est obtenue. Une étude complémentaire d'un sytème NaY préhydratée/benzène (3) est également effectuée. Pour (1), (2) et (3) les rapports BZ(C)/BZ(W) et les répartitions des deux espèces indépendantes d'adsorbat ainsi que les variations du paramètre de la maille cubique sont donnés. Dans (3) deux espèces ordonnées de molécules d'eau WI′ et WII sont trouvées et leurs répartitions décrites. Pour (3) une forte migration cationique est mise en évidence. Dans (2), deux espèces indépendantes et totalement désordonnées de benzène sont trouvées. Il est conclu que la calorimétrie d'adsorption apporte des informations décisives pour la compréhension des mécanismes d'adsorption. ***Pour citer cet article : B.F. Mentzen, C. R. Chimie 8 (2005).***

* Corresponding author.
E-mail address: mentzen.b@infonie.fr (B.F. Mentzen).

1631-0748/$ - see front matter © 2005 Académie des sciences. Publié par Elsevier SAS. Tous droits réservés.
doi:10.1016/j.crci.2004.11.024

Keywords: Faujasite/benzene host–guest complexes; X-ray and neutron powder diffractions; Crystal structure; Adsorption calorimetry; Molecular mechanics simulations

Mots clés : Complexes faujasite/benzène ; Diffractions X et neutroniques sur poudres ; Structure cristalline ; Calorimétrie d'adsorption ; Simulations par mécanique moléculaire

1. Introduction

Microporous materials presenting the faujasite (FAU) structure type [1] are widely involved in many industrial molecular sieving, distillation, detergent-builder or catalytic processes [2,3]. The framework structure of Y-type faujasites usually crystallizes in the cubic Fd3m space group. It is built up by sodalite cages (also called β-cages, centered on 8a positions) linked together by double hexagonal rings (D6R, hexagonal prism, 16c positions). The large cavity (also called super-cage or α-cage, centered on 8b positions) is created by the arrangement of eight sodalite units. Each super-cage communicates with four adjacent super-cages through single twelve-ring windows (S12R, centered on 16d positions) and with four sodalite cages through single six-ring (S6R) windows. Neutron powder diffraction [4] and computational methods [5] show that the ideal cation distribution in anhydrous NaY (Si/Al = 2.43) is 8NaI (in the D6R hexagonal prisms, half- populated 16c positions) +16 NaI′ (in the beta-cages, half-populated 32e positions) +32 Na (in the alpha-cages close to S6R, fully populated 32e positions). Concerning NaY [4,6–13] and other cation-exchanged FAU [14–19], or deluminated Y (DAY or US-Y) [20–22], many experimental and theoretical work [23-27 and many references therein] describing the state of benzene molecules sorbed in these materials are reported in the literature. Nevertheless, there are still some conflicting results concerning the benzene and/or cation distributions, the adsorption heats and the sorption capacities of benzene in NaY and DAY faujasites. Computer simulations by molecular mechanics and molecular dynamics using several force-fields have been widely used for the prediction of preferential adsorption sites of many aromatic and aliphatic species in zeolitic host/guest systems [23–27]. Hereafter it is shown that the van der Waals type Buckingham exp-6-1 atom-atom interaction model combined with crystal structure results have been successfully used for simulating the experimental NaY/benzene and DAY/benzene calorimetric curves. Structural results concerning prehydrated pHyNaY/benzene complexes show that the benzene distributions and cation populations are heavily perturbated by polar water molecules.

2. Experimental

The computer simulation methodology (simplex type variable step method) concerning the charge distributions on the zeolite T(Si,Al) and O framework atoms and the potential energy parameters of the Si,O,C,Na atoms used in this work (Table 1) for the exp-6-1 van der Waals-type Buckingham intermolecular atom–atom potential interaction model (equation 1) are detailed in [28–30].

$$E_{\text{tot}} = \Sigma_{j>k} \left\{ b_j b_k \exp\left[-\left(c_j + c_k \right) r_{jk} \right] - a_j a_k r_{jk}^{-6} + q_j q_k r_{jk}^{-1} \right\} \quad (1)$$

a,*b*,*c* and *q* parameters correspond to the long-range attractive dispersion, short-range repulsion, van der Waals radius and very long-range Coulombic terms respectively. The charges on C/H/Na/O/Si are –0.153/+0.153/+1.0/–*n* *q*(Na)/*m*/0.0 respectively. For the framework oxygen *n* and *m* are the total Na cations and O framework atoms in the simulated structural model respectively. Since this structural model is spherical, it

Table 1
The Buckingham model: atomic potential parameters *a*,*b* and *c* used for the simulations of sorbent/sorbate interactions in the FAU structure type

Atom	*a* (kJ/mol)$^{1/2}$Å^3	*b* (kJ/mol)$^{1/2}$Å^3	*c* (Å^{-1})	Ref.
H	11.662	108.06	1.87	[30]
C	49.132	606.01	1.80	[30]
O	33.211	536.21	1.98	[30]
Si (Al)	66.000	493.00	1.41	[30]
Na	66.000	680.00	1.86	[30]

has been verified that the charges on the Si framework atoms might be neglected. The structural models for the completely dehydrated NaY faujasite and the benzene molecule are reported in [4,31]. All the energy-minimization calculations are performed by using locally developed codes on an AMD Athlon™ Processor (1GHz) based microcomputer. In all cases the calculations are performed by centering the mobile molecule(s) in a spherical zeolitic fragment of 15 or 20 Å radius and the structural parameters correspond to actual data obtained by Rietveld-type refinements [32,33]. High-precision differential molar adsorption calorimetric data on NaY (Si/Al = 2.43) and US-Y (Si/Al = 95) obtained by using a Tian-Calvet type microcalorimeter are described in [10,20]. The NaY zeolite (Si/Al = 2.43) used in this work correponds to a commercial products (Linde Na-Y zeolite SK40 and LZY-52 from Sigma ALDRICH™). The chemical composition of the fully hydrated $Na_{56}Al_{56}Si_{136}O_{384}{\cdot}256H_2O$ zeolite has been verified by elemental analysis, solid state ^{29}Si NMR, water adsorption isotherms and thermogravimetry. The highly siliceous DAY (Si/Al ≈ 200) sample has been obtained by dealumination of a parent silicon-rich Y (Si/Al = 10) refluxed in boiling nitric acid (60% acid/water solution followed by pure acid treatment) (21). The neutron data have been recorded on the D1A (NaY/C_6D_6 phases), D1B (NaY/C_6H_6 phases) and D2B (for one DAY/C_6D_6 sample) powder diffractometers at the Institut Laüe-Langevin in Grenoble (France). The experimental step-scanned X-ray powder diffraction profiles have been recorded on a PHILIPS™ PW1830 X′Pert type diffractometer (different angular ranges, 0.02 or 0.025 steps, 5s counting time/step) using a post-monochromatized (pyrolitic graphite) Cu Kα radiation. For the prehydrated pHyNaY/benzene samples (7.0 weight %, 18 water molecules/unit-cell) a specially designed air-tight brass sample-holder with a Kapton film window has been used and several FAU/benzene compositions have been obtained by injecting through a silicon rubber septum weighted amounts of sorbate. It has been verified that no incomming water or escaping benzene occurred during the data-collections. Some samples have also been packed in glass capillaries and mounted on a basic sample-holder (non-rotating samples). All the data-collections have been recorded at ambient room temperature. In all cases the Fd3m space group has been considered for the structure refinements.

3. Results and discussion

3.1. Structure refinements

The starting crystal parameters for the FAU framework are those given in [4] (*Fd*3*m* space group). In all cases the planar geometry of the benzene species has been constrained to that described in [31,34] for crystals at 270 K (C–C = 1.397, C–H = 1.027 Å, all angles = 120°). In the case of prehydrated NaY/benzene phases (pHyNaY) the starting crystal parameters of the water molecules obtained by computer simulations (see Fig. 3 and section 3.3) are comparable to those reported in [15]. The benzene species close to the NaII cations and those in the S12R windows are labelled BZ(C) and BZ(W) respectively. The water species coordinated to NaI′ and NaII cations are labelled WI′ and WII respectively. The BZ(C)/BZ(W) ratio obtained for the three NaY/benzene, DAY/benzene and pHyNaY/benzene systems are represented in Fig. 1. The unit-cell parameter variations versus benzene loadings for these three systems are given in Fig. 2.

3.1.1. The NaY/benzene system

In this system the variation of the r = BZ(C)/BZ(W) ratio versus benzene loadings is almost linear. Points 1 and 3 are from reference [4], points 2 and 4 correspond to NaY/C_6H_6 (D1B) complexes and point 5 to a sample in a glass capillary (X-rays). The BZ(C)/BZ(W) distributions might be calculated for all loadings by the

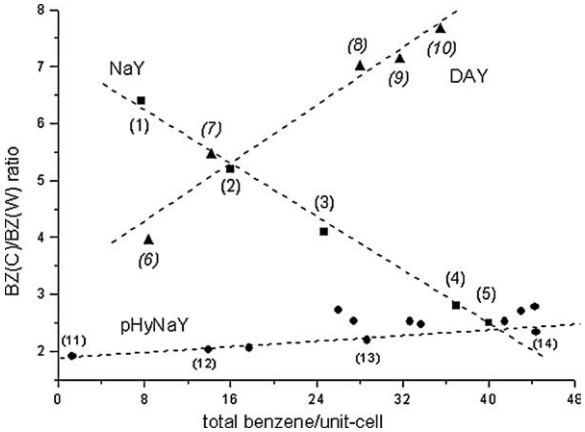

Fig. 1. BZ(C)/BZ(W) ratio versus benzene loadings observed for the three NaY/benzene, prehydrated NaY/benzene and DAY/benzene systems.

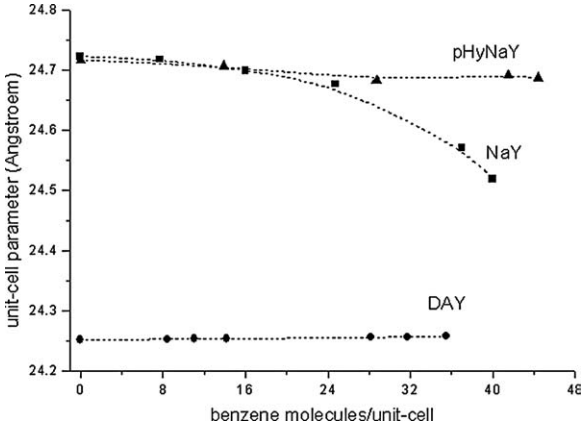

Fig. 2. Unit-cell parameter (Å) versus benzene loadings observed for the three NaY/benzene, prehydrated NaY/benzene and DAY/benzene systems.

$r = 7.235 - 0.122 \times$ (total benzene/uc) ($R = 0.995$). Accordingly, the r ratio decreases with sorbate fillings. At zero filling this ratio is 7.24 (close to 8) and extrapolated to 48 benzene/uc (theoretical maximum) its value is about 1.4. The experimentally observed sorption capacity of benzene in NaY (Si/Al = 2.43) is close to 42–43 molecules/uc (42.5 [10], 43.2 [8]), which roughly corresponds to point 5 with $r \approx 2$. Fig. 2 shows that for this system the unit-cell parameter of the FAU framework decreases rather rapidly with higher benzene loadings. For all benzene loadings the cation site populations remain almost constant [4, this work]. The Rietveld plots and some structural results corresponding to points 2, 4 and 5 are reported in Appendix 1 and Figs. A.I.1 to A.I.3.

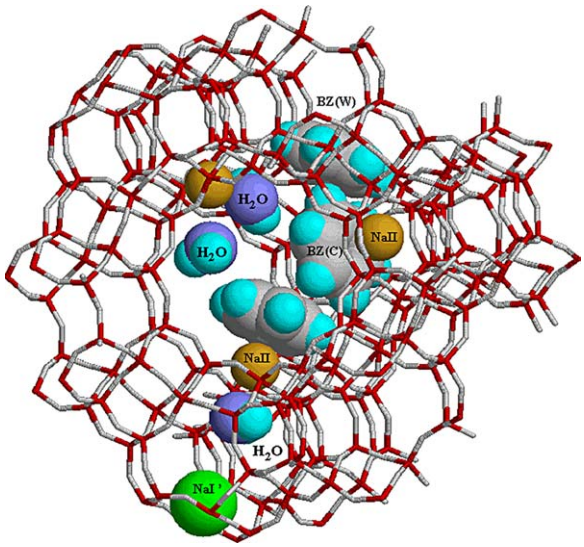

Fig. 3. Structural detail of a prehydrated NaY+24benzene+24water complex (only one eighth of the unit-cell is represented).

3.1.2. The DAY/benzene system

For this system, the r versus fillings ratio increases rapidly with increasing benzene loadings. At saturation (39.5 molecules/uc [20]) the BZ(W) species have almost disappeared. This particularity will be discussed in the sections concerning the calorimetric curve and the computer simulations. The crystal structure corresponding to a DAY/32benzene phase ($r = 7.1$) close to the saturation capacity has been reported in [21]. The corresponding atomic coordinates are reported in Appendix 2 as additional data and the Rietveld plot is given in Fig. A.II.6. Fig. 2 shows that for this system the unit-cell parameter of the FAU framework increases slowly and linearly with increasing benzene loadings. The Rietveld plots, refined benzene molecules and some structural results corresponding to points 6–10 are reported in Appendix 2 and Figs. A.II.1 to A.II.5. Unfortunalety no intermediate benzene loading between points 7 and 8 is presently available.

3.1.3. The pHyNaY/benzene system

For this system, the r versus benzene/uc variation is also linear. For all compositions, r is slightly increasing, its mean value being close to 2. Fig. 2 shows that the unit-cell parameter of the FAU framework decreases slowly and linearly with increasing benzene loadings. The WI′ and WII water molecules have been localized near the NaI′ and NaII cations respectively. Table 2 reports some structural results concerning three pHyNaY/benzene complexes and compares them to the sorbate free NaY. In the present case several details must be emphasized.

At constant water loading (18 molecules/uc):

– **(1)** the Na cation distribution is heavily disturbed; this is a direct result of water/framework and/or water/Na interactions as in prehydrated BaX/xylene phases where cation migrations have also been observed [15];
– **(2)** with increasing benzene concentrations the population of site NaI decreases almost to nil, whereas the population of site NaI′ remains almost constant

Table 2
Distribution of the NaI, NaI′ and NaII cationic species, the BZ(C) and BZ(W) benzene species, and the WI′ and WII water species in three prehydrated pHyNaY/benzene complexes (per unit cell)

Sample	a(Å)	NaI	NaI′	NaII	BZ(C)	BZ(W)	WI′	WII
empty NaY	24.715(1)	8[a]	16	32	0	0	0	0
PL_1.3BZ	24.716	8	17	31	0.85	0.45	0	18
PL_15BZ	24.705(1)	5	25	26	8	7	1	17
PL_29BZ	24.693(1)	3	26	27	19	10	3	15
PL_43BZ	24.690(1)	1	25	30	30	13	8	10

[a] Site population e.s.ds are typically 2–4% of the refined value.

and that of site NaII increases as a consequence of a compensating effect of the decreasing NaI population;
– **(3)** at the same time, the WII site population decreases at the advantage of WI′ coordinated to NaI′ and with increasing benzene loadings some water molecules are forced into the sodalite cage.

Fig. 3 represents an example of a prehydrated pHyNaY/benzene structure for an overall NaY + 24 benzene + 24 water composition: 2BZ(C), 1WI′ and 2WII are coordinated to NaII, NaI′ and NaII respectively, whereas 1BZ(W) is in the plane of the S12R window and its protons interact with framework atoms. The simulated structural models of the WI′ and WII water species are given in section 3.3. The benzene adsorption capacity in prehydrated NaY is very close to that observed for pure NaY (43-44 molecules/uc). The Rietveld plots and some structural results corresponding to four selected points 11-14 are reported in Appendix 3.

3.2. Calorimetric results

The differential molar adsorption heats at 300 K for the NaY/benzene and US-Y/benzene systems are represented in Fig. 4. For the first system, the adsorption heat increases linearly from zero-filling (extrapolated value ≈ –78 kJ/mol) up to 32 benzene/uc (–86 kJ/mol). This corresponds to a mean heat increase of 0.27 kJ/mol per adsorbed benzene molecule and corresponds to Coulombic intermolecular benzene/benzene interactions. After 32 benzene/uc (4 molecules per super cage), the adsorption heat decreases abruptly down to –58 kJ/mol at saturation (42.5 benzene/uc), which corresponds to 5.31 benzene molecules per super cage. The heat decrease corresponds to increasing repulsive interactions between the adsorbed species: even if the theoretical crystal chemical sorption capacity is 48 benzene/uc ([4 BZ(C) + 2BZ(W)] per super cage), at this concentration there is not enough place for so much sorbate. For the US-Y/benzene system the situation is much more complicated. The US-Y sample corresponds to Si/Al = 95 [10] and contains still 2 Na cations per unit-cell. These residual cations and unavoidable structural defects provoked by the dealumination process itself may play a specific role in the starting adsorption process and therefore the initial heats are rather high: the initial curve might be extrapolated at zero filling and compared to the NaY/benzene initial heat (–78 kJ/mol). Accordingly, the first data points of the US-Y/benzene curve should be discarded and the true initial adsorption heat be extrapolated to about –42 kJ/mol. Up to 12 benzene/uc the mean heat increment is about 0.29 kJ/mol and from 12 up to 20 benzene/uc it is 0.75 kJ/mol, the maximum heat being –52.5 kJ/mol. After 20 benzene/uc the heat decreases down to –41 kJ/mol, the mean decrement being 0.96 kJ/mol. Finally, up to saturation (39.5 ben-

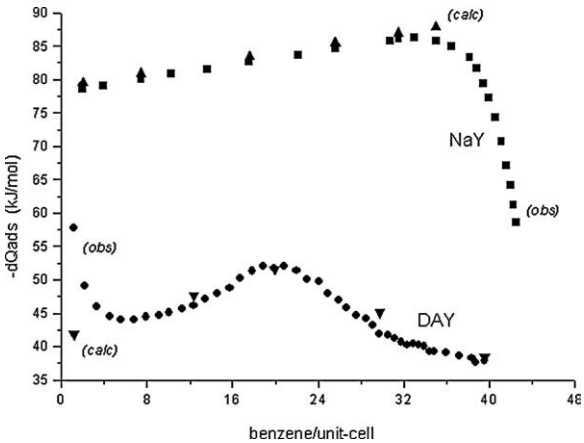

Fig. 4. Experimental differential molar adsorption heat curves at 300K for the NaY/benzene [20] and US–Y/benzene systems [10].

zene/uc or 4.94 benzene per super cage) the heat decrement is about 0.36 kJ/mol, the minimum adsorption heat being –37.5 kJ/mol. For this system the benzene condensation heat is almost attained (–33.5 kJ/mol at 300 K).

3.3. Computer simulations

3.3.1. The NaY/benzene system

Energy-minimization calculations using the exp-6-1 Buckingham model yield –79.0 and –46.7 kJ/mol for the adsorption heats of isolated BZ(C) and BZ(W) species at infinite dilution respectively [30]. The relatively large difference between these energies explains why at lower loadings the cationic site is favoured. This is in agreement with the r ratio line and the crystal structure refinements [4, this work]. It has been verified that at all loadings the benzene locations and orientations remain the same [4, this work]. This is a direct consequence of the specific BZ(C)/cation and BZ(W)/framework interactions. Knowing the distributions of the two types of benzene species for all loadings, the estimated adsorption heats for points 1 to 4 in Fig. 1 have been estimated. The benzene/benzene interactions between BZ(C)/BZ(C), BZ(C)/BZ(W) and BZ(W)/BZ(W) have been calculated for increasing benzene species in a spherical faujasite structural moeity centered on the super cage (x,x,x = 3/8) with 20Å radius. The mean BZ/BZ interaction increment for increasing loadings amounts to 0.252 kJ/mol, which is in correct agreement with the experimentally observed 0.27 kJ/mol value. The calculated values (triangular ▲ and ▼symbols) are compared to the experimental adsorption heats in Table 3 and reported in Fig. 4. After 32 benzene/uc the unit-cell parameter decreases (Fig. 2) and at the same time the adsorption heat drops. This rapid decrease of the adsorption heats might be the consequence of simultaneaous effects due (**a**) to increas-

Table 3
Observed and calculated adsorption heats for four NaY/benzene fillings

Point	BZ(C)/BZ(W) ratio	Benzene/uc	$-E_{obs}$ (kJ/mol)	$-E_{cal}$ (kJ/mol)	
1	6.4	7.7	80	80.9	
2	5.2	16.0	82	83.0	
3	4.1	24.7	84		85.2
4	3.3	37.0	86		87.1

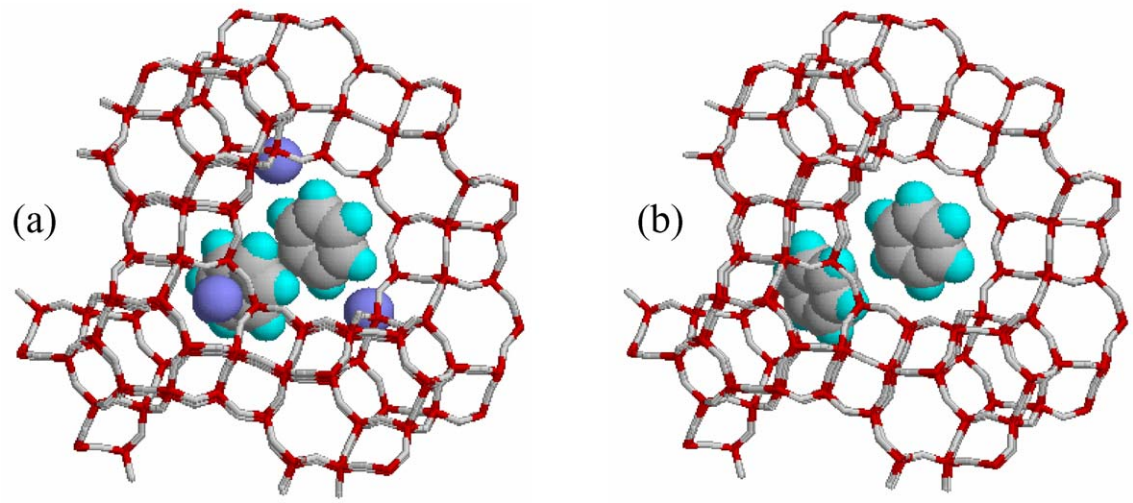

Fig. 5. The two independent benzene molecules in (**a**) NaY and (**b**) DAY at infinite dilution.

ing unfavourable benzene/ benzene interactions as a consequence of unit-cell volume decrease, (**b**) to increasing concentrations of the BZ(W) species which present much lower adsorption heat contributions and (**c**) to the end of the pore-filling effect.

3.3.2. The US-Y/benzene system

There are no adsorption heats available for the DAY/benzene system (Si/Al ≈ 200). The only comparable data are those reported in [10] and represented in Fig. 4 (Si/Al = 95). Fig. 5a,b compare the locations of the two independent benzene species in NaY and DAY. These locations correspond to isolated species at zero filling. For DAY the calculated adsorption heats for BZ(C) and BZ(W) are –41.2 and –35.9 kJ/mol respectively. The extrapolated experimental value at zero filling is about –42 kJ/mol. The calculated heats for both benzene species are very close. Accordingly, we might expect that both sites are equally probable. The r line for this system shows that at increasing benzene fillings the BZ(W) species is less and less favoured: in other terms, everything happens as if the BZ(W) species progressively vanish at higher loadings. In fact, the structure refinements and the simulations show that when the two benzene species coexist, BZ(W) quits the S12R window and gets closer to BZ(C): the non-interacting molecules in Fig. 5b yield those represented in Fig. 6a when both benzene species interact. The starting structural models for the BZ(C) and BZ(W) benzene species in DAY which have been simulated by molecular mechanics are given in Table 4. These positions are very close to those reported for DAY/benzene complexes analyzed by neutron powder diffraction (see Appendix 2 and the results corresponding to Figs. A.II.1 and A.II.6). It might be preferable to label the two independent sorbate species BZ1 and BZ2, but for homogeinity with the NaY/benzene and pHyNaY/benzene systems we still label them BZ(C) and BZ(W). The energy-minimization calculations show that the benzene/benzene interactions are much higher than in the NaY/benzene system, where the benzene species could not quit their sorption sites. Fig. 6 shows some benzene distributions for 2,3,4 and 5 benzene/super cage respectively. The calculated benzene/benzene mean interaction increment up to 20 benzene/uc amounts to 0.59 kJ/mol and at higher loadings up to saturation there is a decrement of about 0.67 kJ/mol. For comparison, the experimentally observed mean increment and decrement are 0.52 and 0.66 respectively. The benzene sorption capacity of US-Y is 39.5 molecules/uc. Since there are no Na cations in US-Y, the BZ(C) are closer to the framework and in greater confinement. As a consequence the centre of the alpha cage is able to accept a benzene molecule, the result being the formation a $(C_6H_6)_5$ cluster (Fig. 6d) at 40 benzene/uc, which is comparable to the saturation capacity of US-Y. Compared to NaY/benzene, where the sorbate species are fully ordered, in DAY/benzene they are completely disordered at room temperature. Accordingly, the distributions represented in Fig. 6a,b,c,d are some among an infinity of possible solutions.

Table 4
Modelisation of isolated BZ(C) and BZ(W) in DAY by molecular mechanics

BZ(C)				BZ(W)			
C11	.3187	.4076	.2226	C21	.5348	.4641	.4745
C12	.3245	.3014	.2668	C22	.4671	.5378	.5316
C13	.2767	.3884	.2571	C23	.4983	.4980	.4456
C14	.3665	.3206	.2323	C24	.5036	.5039	.5605
C15	.2796	.3353	.2792	C25	.4644	.5348	.4741
C16	.3636	.3737	.2103	C26	.5375	.4671	.5319
H11	.3166	.4467	.2061	H21	.5597	.4370	.4535
H12	.3266	.2623	.2830	H22	.4423	.5649	.5526
H13	.2437	.4133	.2662	H23	.4963	.4968	.4033
H14	.3995	.2956	.2232	H24	.5056	.5061	.6027
H15	.2488	.3212	.3044	H25	.4376	.5598	.4529
H16	.3944	.3878	.1849	H26	.5643	.4421	.5532

3.3.3. The pHyNaY/benzene system

The atomic coordinates of the adsorbed WI′ and WII water species simulated by molecular mechanics are gien in Table 5. In order to avoid undesired parameter correlations, these coordinates together with the known benzene coordinates have been fixed during the refine-

Table 5
Modelisation of isolated WI′ and WII in pHyNaY by molecular mechanics

WI′				WII			
Ow1	.1668	.1672	.1708	Ow2	.2111	.3246	.3286
Hw11	.1807	.1345	.1914	Hw21	.1710	.3307	.3227
Hw12	.1340	.1825	.1901	Hw22	.2214	.3375	.3662

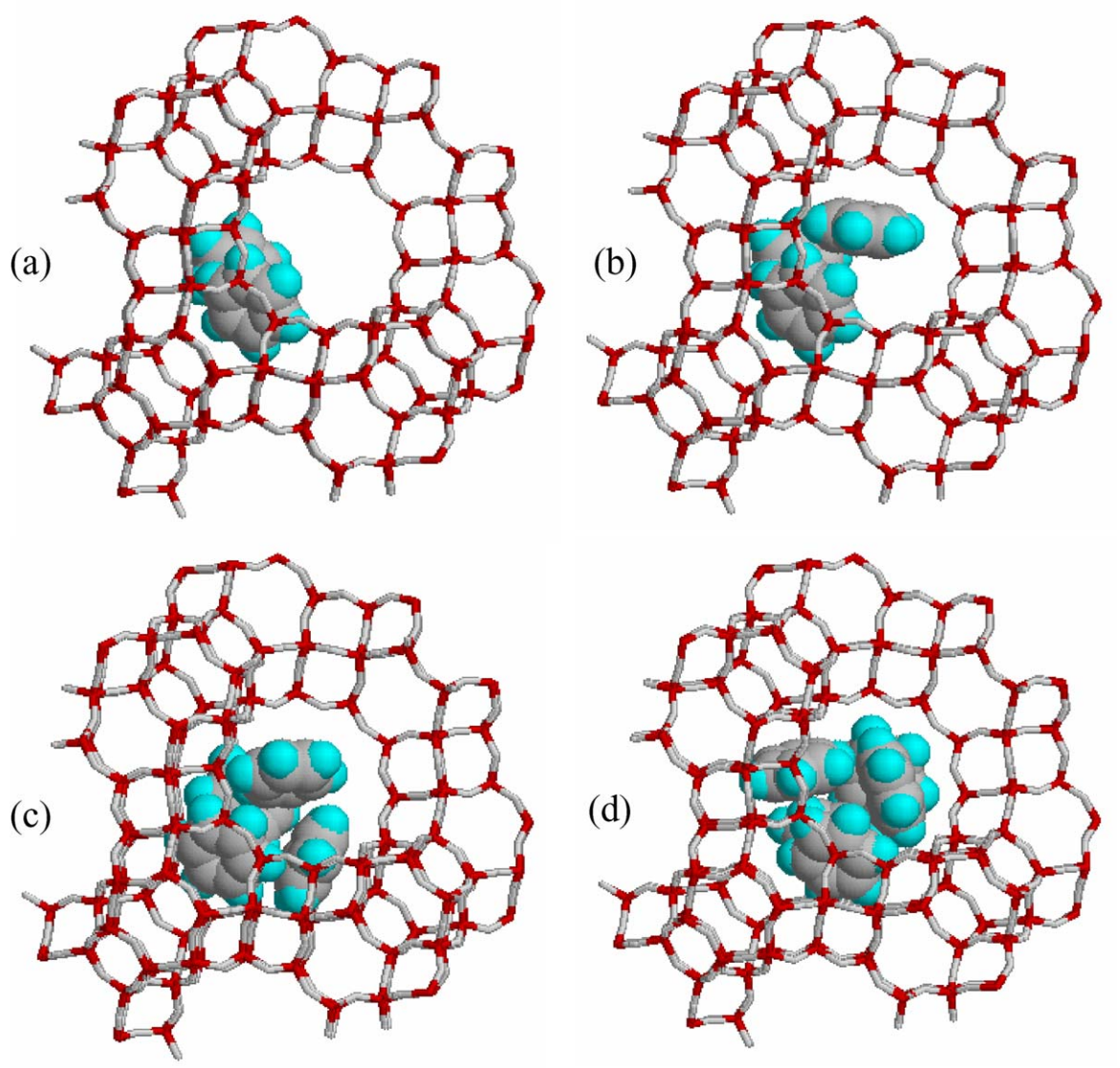

Fig. 6. Computer simulation of the DAY/benzene system: possible benzene distributions at (**a**) 2, (**b**) 3, (**c**) 4 and (d) 5 benzene/super cage.

ment process and only their populations have been relaxed.

4. Conclusion

It appears that the benzene adsorption process in faujasite type zeolites drastically depends on the starting material. The preference of the benzene molecules for a cationic or a window site is very different in NaY and DAY. The comparison of structural results, experimental calorimetric curves and van der Waals type computer simulations yields a better knowledge on the intimate mechanism of benzene adsorption in faujasite. Some details of this mechanism could only

be attained by the interpretation of the calorimetric curve. Therefore, whenever possible, structural and calorimetric investigations should be performed on the same sample, since small variations in the chemical composition or the presence of residual cations, which are not easely detected by diffraction techniques, might be revealed by the differential molar adsorption heat curve. In order to illustrate the specific role of a polar molecule on the benzene adsorption process in NaY, a prehydrated NaY/benzene system has also been investigated. It appears that in this system the benzene distribution over the cationic and window sites is almost constant at all fillings. With increasing sorbate amounts the water molecules coordinated to the NaII cation are progressivley forced into the sodalite cage where the benzene molecules do not penetrate, the sorption capacities of the pure NaY and the prehydrated NaY being almost the same. The most important result of water/benzene coadsorption is the dramatic cationic migration effect: at constant water content (about 18 molecules/uc) the NaI cations migrate completely into the sodalite cage.

Appendix 1 – Points 1 to 5 in Fig. 1 for the NaY/benzene system. Points 1 and 3 are given in ref. [4]

In all cases: upper/medium/lower traces correspond to calculated/experimental/difference plots

Point 2

Sample label: NA56YBZ
Sample formula: $Na_{56}Al_{56}Si_{136}O_{384}$·***16*** C_6H_6
Sample origin: Linde sodium-Y zeolite (see ref. [4]) in Al-tube
Diffractometer: D1B – ILL
Wavelength (Å): 2.5224
Angular range (°2θ): 7.0 – 83.6 (limited data-collection)
Angular step (°2θ): 0.2
Unit-cell parameter (Å): 24.699(4)
Number of observables: 384 + 37 = 421
Number of *hkl* triplets: 73
$R_p/R_{wp}/R_{ex}/R_I$ (%): 9.9/16.0/1.9/8.2

Atom	*x/a*	*y/b*	*z/c*	*B* (iso)	population/uc
Si	–.0544(5)	.0351(6)	.1244(5)	0.8	192
O1	–.1090(5)	0	.1090(5)	2.5	96
O2	–.0028(5)	–.0028(5)	.1418(7)	2.5	96
O3	–.0343(8)	.0714(5)	.0714(5)	2.5	96
O4	–.0684(8)	.0758(5)	.1742(5)	2.5	96
NaI	0	0	0	3.3	8(1)
NaI’	.055(3)				16(1)
NaII	.236(2)				32(1)
C1	.257	.337	.297	9.0	13.4(6)
H1	.226	.368	.297		
C2	.477	.477	.546	9.0	2.6(5)
H2	.459	.459	.582	9.0	

Si–O1 1.641(2) Si–O2 1.631(2) Si–O3 1.653(2) Si–O4 1.618(2)

Benzene geometries and coordinates, total Na/uc and thermal parameters fixed (see [4]).

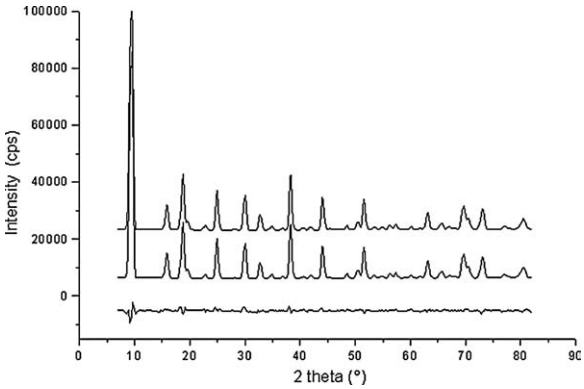

Fig. A.I.1. Rietveld plots for $Na_{56}Al_{56}Si_{136}O_{384}$·***16*** C_6H_6 (point 2 in Fig. 1).

Point 4

Sample label: L52ALBZ
Sample formula: $Na_{56}Al_{56}Si_{136}O_{384}$·***37*** C_6H_6
Sample origin: LZY-52 (sigma Aldrich) in Al tube
Diffractometer: D1B – ILL
Wavelength (Å): 2.5224
Angular range (°2θ): 7.0–82.0 (limited data-collection)
Angular step (°2θ): 0.2
Unit-cell parameter (Å): 24.570(4)
Number of observables: 376 + 37 = 413
Number of *hkl* triplets: 73
$R_p/R_{wp}/R_{ex}/R_I$ (%): 10.2/16.4/2.0/7.9

Atom	x/a	y/b	z/c	B(iso)	population/uc
Si	–.0541(4)	.0355(4)	.1242(4)	0.8	192
O1	–.1086(3)	0	.1086(3)	2.5	96
O2	–.0024(4)	–.0024(5)	.1435(7)	2.5	96
O3	–.0354(7)	.0708(4)	.0708(4)	2.5	96
O4	–.0719(7)	.0759(4)	.1741(4)	2.5	96
NaI	0	0	0	3.3	8(1)
NaI'	.059(4)				16(1)
NaII	.238(2)				32(1)
C1	.257	.337	.297	9.0	27.0(7)
H1	.226	.368	.297		
C2	.477	.477	.546	9.0	9.8(5)
H2	.459	.459	.582	9.0	

Si–O1 1.654(2) Si–O2 1.657(2) Si–O3 1.650(2) Si–O4 1.650(2)

Benzene geometries and coordinates, total Na/uc and thermal parameters fixed (see [4]).

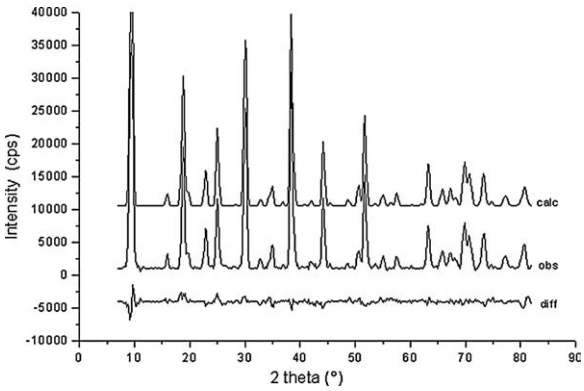

Fig. A.I.2. Rietveld plots for $Na_{56}Al_{56}Si_{136}O_{384}\cdot\boldsymbol{37}C_6H_6$ (point 4 in Fig. 1).

Point 5

Sample label: cpY56BZ2
Sample formula: $Na_{56}Al_{56}Si_{136}O_{384}\cdot\boldsymbol{40}\ C_6H_6$
Sample origin: LZY-52 (Sigma Aldrich) in glass capillary
Diffractometer: Philips – X′Pert
Wavelength (Å): Cu Kα
Angular range (°2θ): 4.0 – 84.0
Angular step (°2θ): 0.025
Unit-cell parameter (Å): 24.518(4)
Number of observables: 3201 + 37 = 3238
Number of *hkl* triplets: 282
$R_p/R_{wp}/R_{ex}/R_I$ (%): 5.8/7.6/7.7/13.1

Atom	*x/a*	*y/b*	*z/c*	*B*(iso)	population/uc
Si	–.0532(2)	.0357(2)	.1261(2)	0.8	192
O1	–.1066(2)	0	.1066(2)	2.5	96
O2	–.0017(2)	–.0017(2)	.1443(4)	2.5	96
O3	–.0344(4)	.0746(2)	.0746(2)	2.5	96
O4	–.0729(4)	.0727(2)	.1773(2)	2.5	96
NaI	0	0	0	3.3	8(1)
NaI'	.0625(9)				16(1)
NaII	.2359(6)				32(1)
C1	.257	.337	.297	9.0	28.5(5)2)
H1	.226	.368	.297		
C2	.477	.477	.546	9.0	11.4(2)
H2	.459	.459	.582	9.0	

Si–O1 1.655(4) Si–O2 1.631(6) Si–O3 1.657(5) Si–O4 1.631(5)

Benzene geometries and coordinates, total Na/uc and thermal parameters fixed (see [4]).

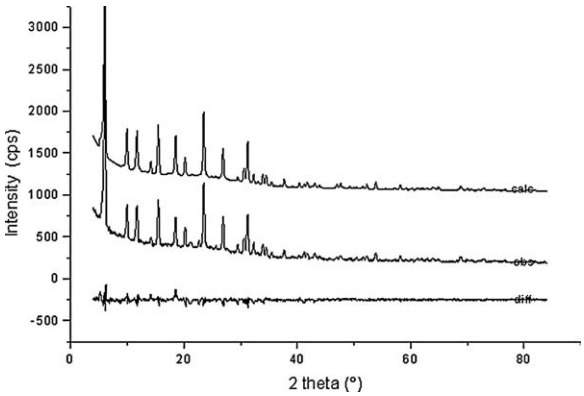

Fig. A.I.3. Rietveld plots for $Na_{56}Al_{56}Si_{136}O_{384}\cdot\boldsymbol{40}\ C_6H_6$ (point 5 in Fig. 1).

Appendix 2 – Points 6 to 10 in Fig. 1 for the DAY/benzene system

DAY/benzene complex at lower loading

Point 6

Sample label: Y20a_bz1
Sample formula: $Si_{192}O_{384}\cdot 8.4\ C_6D_6$
Sample origin: see text
Diffractometer: D2B – ILL quartz tube
Wavelength (Å): 1.59263
Angular range (°2θ): 4.55–106.55
Angular step (°2θ): 0.05
Unit-cell parameter (Å): 24.252
Number of observables: 2201 + 94 = 2295

Number of *hkl* triplets: 407
$R_p/R_{wp}/R_{ex}/R_I$ (%): 5.5/7.0/8.5/10.4

Atom	*x/a*	*y/b*	*z/c*	*B* (iso)	population/uc
Si	–.0541(1)	.0359(2)	.1251(1)	0.61(9)	192
O1	–.1065(1)	0	.1065(1)	1.0(2)	96
O2	–.0038(1)	–.0038(1)	.1403(2)	0.8(2)	96
O3	–.0358(2)	.0762(1)	.0762(1)	2.3(2)	96
O4	–.0705(3)	.0712(2)	.1722(2)	1.9(2)	96
C11	.3274(9)	.4114(4)	.2345(9)	10(2)	6.7(2)
C12	.328(2)	.3032(7)	.233(3)		
C13	.293(2)	.3964(6)	.278(3)		
C14	.367(2)	.3200(8)	.235(2)		
C15	.292(1)	.3419(5)	.296(1)		
C16	.368(1)	.3750(6)	.217(2)		
D11	.326(2)	.4518(6)	.222(2)		
D12	.329(3)	.263(1)	.285(4)		
D13	.266(2)	.4232(7)	.297(3)		
D14	.396(4)	.294(2)	.219(5)		
D15	.263(3)	.327(1)	.324(3)		
D16	.397(3)	.389(1)	.189(3)		
C21	.549(1)	.476(2)	.471(1)	15(3)	1.7(1)
C22	.487(1)	.557(1)	.526(1)		
C23	.501(1)	.498(1)	.446(1)		
C24	.535(1)	.536(1)	.550(1)		
C25	.469(1)	.537(1)	.474(1)		
C26	.566(1)	.496(1)	.522(1)		
D21	.572(2)	.449(3)	.449(1)		
D22	.467(2)	.589(2)	.544(2)		
D23	.591(1)	.489(2)	.406(1)		
D24	.551(1)	.553(2)	.585(1)		
D25	.431(1)	.548(2)	.460(1)		
D26	.598(2)	.476(2)	.541(1)		

Si–O1 1.603(4) Si–O2 1.598(3) Si–O3 1.599(3) Si–O4 1.608(4)

Benzene geometries constrained (see text).

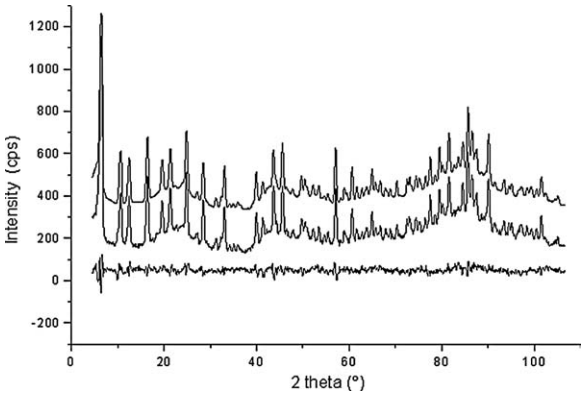

Fig. A.II.1. Rietveld plots for $Si_{192}O_{384}$·***8.4*** C_6D_6 (point 6 in Fig. 1).

Point 7

Sample label: Y20a_bz10
Sample formula: $Si_{192}O_{384}$·14.2 C_6H_6
Sample origin: see text
Diffractometer: Philips – X′Pert – in air-tight brass sample-holder
Wavelength (Å): Cu Kα
Angular range (°2θ): 4–80
Angular step (°2θ): 0.025
Unit-cell parameter (Å): 24.253(1)
Number of observables: 3041 + 94 = 3135
Number of *hkl* triplets: 221
$R_p/R_{wp}/R_{ex}/R_I$ (%): 9.3/12.2/2.6/9.8

Atom	*x/a*	*y/b*	*z/c*	*B* (iso)	population/uc
Si	–.0544(2)	.0354(3)	.1256(3)	0.8	192
O1	–.1076(3)	0	.1076(3)	2.5	96
O2	–.0038(4)	–.0038(4)	.1397(6)	2.5	96
O3	–.0385(6)	.0753(4)	.0753(4)	2.5	96
O4	–.0709(6)	.0711(4)	.1789(4)	2.5	96
BZ(C)	see neutron results			9.0	12.0(3)
BZ(W)				9.0	2.2(3)

Si–O1 1.609(3) Si–O2 1.590(3) Si–O3 1.606(3) Si–O4 1.606(3)

Benzene coordinates fixed to those obtained by neutron profile refinements. Thermal parameters fixed.

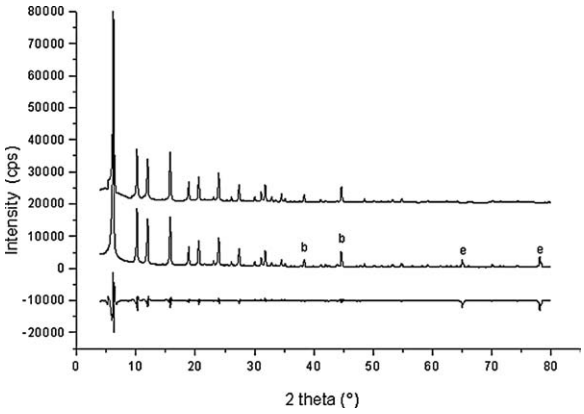

Fig. A.II.2. Rietveld plots for $Si_{192}O_{384}$·***14*** C_6H_6 (point 7 in Fig. 1).

Point 8

Sample label: Y20a_bz100
Sample formula: $Si_{192}O_{384}$·28 C_6H_6
Sample origin: see text
Diffractometer: Philips – X′Pert – in air-tight brass sample-holder
Wavelength (Å): Cu Kα

Angular range (°2θ): 4–77.4
Angular step (°2θ): 0.025
Unit-cell parameter (Å): 24.254(1)
Number of observables: 2937 + 94 = 3031
Number of *hkl* triplets: 225
$R_p/R_{wp}/R_{ex}/R_I$ (%): 7.5/9.6/3.0/8.5

Atom	*x/a*	*y/b*	*z/c*	*B* (iso)	population/uc
Si	–.0530(2)	.0361(2)	.1243(2)	0.8	192
O1	–.1048(3)	0	.1048(3)	2.5	96
O2	–.0012(3)	–.0012(3)	.1421(5)	2.5	96
O3	–.0317(5)	.0777(3)	.0777(3)	2.5	96
O4	–.0706(4)	.0718(3)	.1782(3)	2.5	96
BZ(C)	see neutron results			9.0	24.5(5)
BZ(W)				9.0	3.5(2)

Si–O1 1.602(3) Si–O2 1.608(3) Si–O3 1.601(3) Si–O4 1.620(3)

Benzene coordinates fixed to those obtained by neutron profile refinements. Thermal parameters fixed.

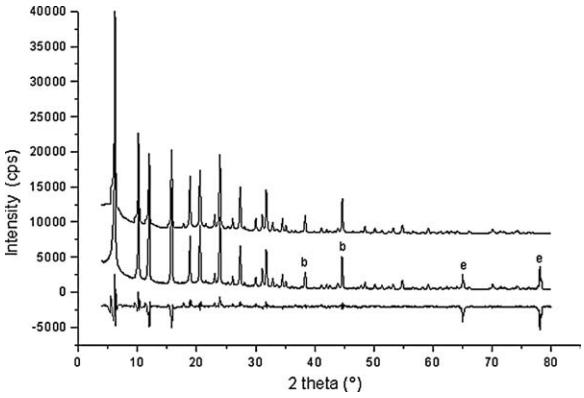

Fig. A.II.3. Rietveld plots for $Si_{192}O_{384}$·28 C_6H_6 (point 8 in Fig. 1).

Point 9

Sample label: Y20a_bz20
Sample formula: $Si_{192}O_{384}$·31.7 C_6H_6
Sample origin: see text
Diffractometer: Philips – X′Pert – in air-tight brass sample-holder
Wavelength (Å): Cu Kα
Angular range (°2θ): 4–80
Angular step (°2θ): 0.025
Unit-cell parameter (Å): 24.256(1)
Number of observables: 3041 + 94 = 3135
Number of *hkl* triplets: 244
$R_p/R_{wp}/R_{ex}/R_I$ (%): 8.4/11.1/2.7/8.5

Atom	*x/a*	*y/b*	*z/c*	*B* (iso)	population/uc
Si	–.0538(3)	.0359(3)	.1260(3)	0.8	192
O1	–.1060(4)	0	.1060(4)	2.5	96
O2	–.0030(4)	–.0030(4)	.1429(6)	2.5	96
O3	–.0385(6)	.0764(4)	.0764(4)	2.5	96
O4	–.0699(6)	.0707(4)	.1793(4)	2.5	96
BZ(C)	see neutron results			9.0	27.8(3)
BZ(W)				9.0	3.9(3)

Si–O1 1.612(3) Si–O2 1.604(3) Si–O3 1.597(3) Si–O4 1.593(3)

Benzene coordinates fixed to those obtained by neutron profile refinements. Thermal parameters fixed.

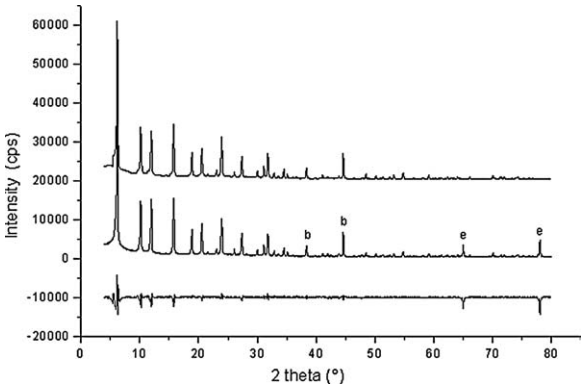

Fig. A.II.4. Rietveld plots for $Si_{192}O_{384}$·***31.7*** C_6H_6 (point 9 in Fig. 1).

Point 10

Sample label: Y20a_bz30
Sample formula: $Si_{192}O_{384}$·35.5 C_6H_6
Sample origin: see text
Diffractometer: Philips – X′Pert – in air-tight brass sample-holder
Wavelength (Å): Cu Kα
Angular range (°2θ): 4–80
Angular step (°2θ): 0.025
Unit-cell parameter (Å): 24.257(1)
Number of observables: 3041 + 94 = 3135
Number of *hkl* triplets: 222
$R_p/R_{wp}/R_{ex}/R_I$ (%): 8.1/10.6/2.7/9.5

Atom	*x/a*	*y/b*	*z/c*	*B* (iso)	population/uc
Si	–.0536(2)	.0356(2)	.1257(2)	0.8	192
O1	–.1055(4)	0	.1055(4)	2.5	96
O2	–.0030(4)	–.0030(4)	.1440(6)	2.5	96
O3	–.0398(6)	.0774(4)	.0774(4)	2.5	96
O4	–.0702(6)	.0701(4)	.1799(4)	2.5	96
BZ(C)	see neutron results			9.0	31.4(3)
BZ(W)				9.0	4.1(2)

Si–O1 1.603(3) Si–O2 1.606(3) Si–O3 1.590(3) Si–O4 1.611(3)

Benzene coordinates fixed to those obtained by neutron profile refinements. Thermal parameters fixed.

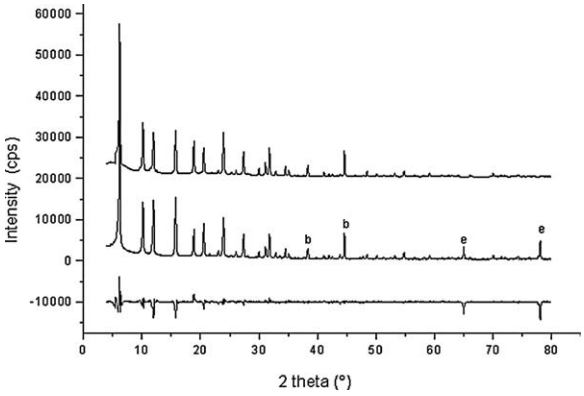

Fig. A.II.5. Rietveld plots for $Si_{192}O_{384}$·***35.5*** C_6H_6 (point 10 in Fig. 1).

DAY/benzene complex at higher loading

Additional data (compare with sample of point 6)
Sample label: Y20a_BZ600
Sample formula: $Si_{192}O_{384}$·32 C_6D_6
Sample origin: see text
Diffractometer: D2B
Wavelength (Å): 1.59263
Angular range (°2θ): 4.55–154.35
Angular step (°2θ): 0.05
Unit-cell parameter (Å): 24.253(1)
Number of observables: 2997 + 94 = 3091
Number of *hkl* triplets: 702
$R_p/R_{wp}/R_{ex}/R_I$ (%): 7.9/10.2/7.3/11.2

Atom	*x/a*	*y/b*	*z/c*	*B* (iso)	population/uc
Si	–.0539(2)	.0355(2)	.1254(2)	0.98(9)	192
O1	–.1063(2)	0	.1063(2)	1.4(2)	96
O2	–.0032(2)	–.0032(2)	.1409(3)	1.5(2)	96
O3	–.0365(3)	.0758(2)	.0758(2)	1.4(2)	96
O4	–.0706(3)	.0709(2)	.1791(2)	1.3(2)	96
C11	.3227(8)	.4084(6)	.229(1)	20(2)	27.8(5)
C12	.337(1)	.3078(8)	.283(1)		
C13	.283(2)	.390(2)	.266(3)		
C14	.373(1)	.3232(9)	.241(1)		
C15	.2908(7)	.3406(7)	.295(1)		
C16	.3698(5)	.3768(5)	.219(1)		
D11	.321(1)	.448(1)	.216(2)		
D12	.340(2)	.269(1)	.299(3)		
D13	.248(2)	.413(2)	.273(4)		
D14	.406(2)	.299(1)	.231(3)		
D15	.259(1)	.324(1)	.317(2)		
D16	.4040(8)	.3948(7)	.202(2)		
C21	.549(2)	.477(2)	.470(1)	15(4)	3.9(3)
C22	.487(1)	.558(2)	.525(1)		
C23	.507(1)	.506(1)	.443(1)		
C24	.535(1)	.536(1)	.549(1)		
C25	.473(1)	.542(2)	.472(1)		
C26	.563(2)	.493(3)	.523(2)		
D21	.567(3)	.444(3)	.452(2)		
D22	.468(3)	.589(3)	.544(2)		
D23	.594(2)	.493(2)	.404(1)		
D24	.552(2)	.554(2)	.583(2)		
D25	.437(2)	.556(3)	.455(2)		
D26	.596(4)	.475(4)	.542(3)		

Si–O1 1.602(3) Si–O2 1.591(3) Si–O3 1.606(3) Si–O4 1.610(3)

Benzene geometries constrained (see text)

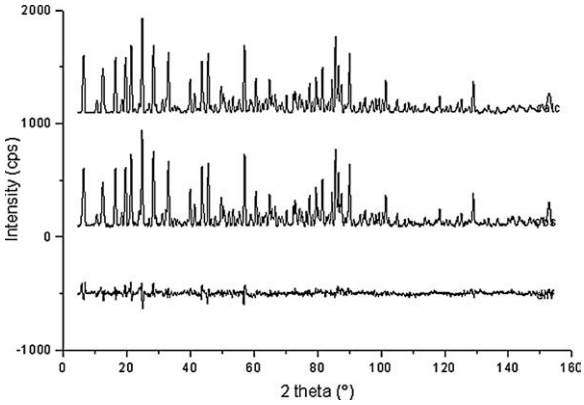

Fig. A.II.6. Rietveld plots for $Si_{192}O_{384}$·***32*** C_6D_6.

Appendix 3 – Points 11 to 14 in Fig. 1 for the pre-hydrated pHyNaY/benzene system

Point 11

Sample label: PL52_A10
Sample formula: $Na_{56}Al_{56}Si_{136}O_{384}$·1.3 C_6H_6 + 18 H_2O
Sample origin: LZY-52 (Sigma–Aldrich)
Diffractometer: Philips – X′Pert – in air-tight brass sample-holder
Wavelength (Å): Cu Kα
Angular range (°2θ): 4–66
Angular step (°2θ): 0.025
Unit-cell parameter (Å): 24.716(1)
Number of observables: 2481 + 16 = 2497
Number of *hkl* triplets: 165
$R_p/R_{wp}/R_{ex}/R_I$ (%): 6.5/9.0/3.5/7.5

Atom	*x/a*	*y/b*	*z/c*	*B* (iso)	population/uc
Si	–.0540(3)	.0353(3)	.1247(3)	0.8	192
O1	–.1073(4)	0	.1073(4)	2.5	96
O2	–.0023(4)	.0023(4)	.1438(6)	2.5	96
O3	–.0330(7)	.0755(4)	.0755(4)	2.5	96
O4	–.0713(6)	.0715(4)	.1785(4)	2.5	96
NaI	0	0	0	3.3	8(1)
NaI'	.0614(7)				17(1)
NaII	.2342(5)				31(1)
C1	.258	.338	.298	9.0	0.85(8)
H1	.227	.369	.298	9.0	
C2	.477	.477	.546	9.0	0.45(5)
H2	.459	.459	.582	9.0	
OW1	.167	.167	.171	9.0	0(1)
H11	.181	.134	.191	9.0	
H21	.134	.181	.191	9.0	
OW2	.211	.326	.326	9.0	18(1)
H21	.171	.331	.323	9.0	
H22	.221	.337	.366	9.0	

Si–O1 1.638(3) Si–O2 1.650(3) Si–O3 1.653(3) Si–O4 1.658(3)

Benzene coordinates, total Na/uc and thermal parameters fixed (see [4]). Water coordinates fixed according to MM simulations (see Tables 4 and 5).

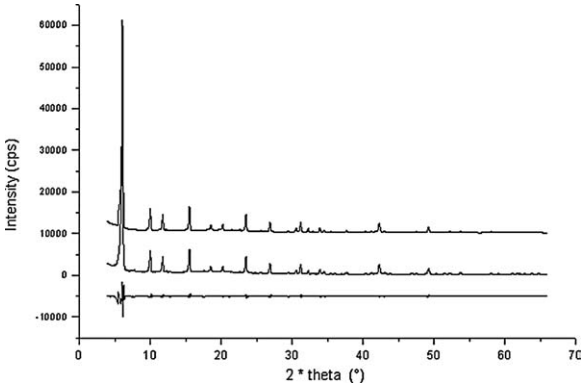

Fig. A.III.1. Rietveld plots for $Na_{56}Al_{56}Si_{136}O_{384}$·***1.3*** C_6H_6 + ***18*** H_2O

Point 12

Sample label: PL52_BZ10

Sample formula: $Na_{56}Al_{56}Si_{136}O_{384}$·15 C_6H_6 + 18 H_2O

Sample origin: LZY-52 (Sigma–Aldrich)

Diffractometer: Philips – X′Pert – in air-tight brass sample-holder

Wavelength (Å): Cu Kα

Angular range (°2θ): 4–66

Angular step (°2θ): 0.025

Unit-cell parameter (Å): 24.705(1)

Number of observables: 2481 + 16 = 2497

Number of *hkl* triplets: 165

$R_p/R_{wp}/R_{ex}/R_I$ (%): 6.0/8.4/3.4/6.5

Atom	*x/a*	*y/b*	*z/c*	*B* (iso)	population/uc
Si	–.0540(3)	.0353(3)	.1247(3)	0.8	192
O1	–.1073(4)	0	.1073(4)	2.5	96
O2	–.0023(4)	–.0023(4)	.1438(6)	2.5	96
O3	–.0330(7)	.0755(4)	.0755(4)	2.5	96
O4	–.0713(6)	.0715(4)	.1785(4)	2.5	96
NaI	0	0	0	3.3	5(1)
NaI'	.0679(9)				25(1)
NaII	.2395(6)				26(1)
C1	.258	.338	.298	9.0	8.1(5)
H1	.227	.369	.298	9.0	
C2	.477	.477	.546	9.0	6.9(5)
H2	.459	.459	.582	9.0	
OW1	.167	.167	.171	9.0	1(1)
H11	.181	.134	.191	9.0	
H21	.134	.181	.191	9.0	
OW2	.211	.326	.326	9.0	17(1)
H21	.171	.331	.323	9.0	
H22	.221	.337	.366	9.0	

Si–O1 1.648(3) Si–O2 1.667(3) Si–O3 1.644(3) Si–O4 1.621(3)

Benzene coordinates, total Na/uc and thermal parameters fixed (see [4]). Water coordinates fixed according to MM simulations.

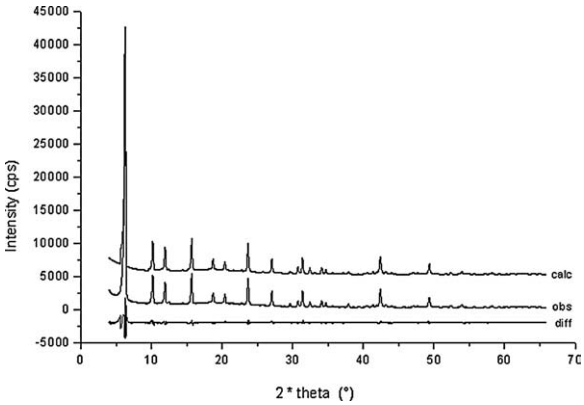

Fig. A.III.2. Rietveld plots for $Na_{56}Al_{56}Si_{136}O_{384}$·***15*** C_6H_6 + ***18*** H_2O (point12 in Fig. 1).

Point 13

Sample label: PL52_BZ20

Sample formula: $Na_{56}Al_{56}Si_{136}O_{384}$·29 C_6H_6 + 18 H_2O

Sample origin: LZY-52 (Sigma – Aldrich)

Diffractometer: Philips – X′Pert – in air-tight brass sample-holder

Wavelength (Å): Cu Kα

Angular range (°2θ): 4–66

Angular step (°2θ): 0.025

Unit-cell parameter (Å): 24.693(1)

Number of observables: 2481 + 16 = 2497

Number of *hkl* triplets: 165

$R_p/R_{wp}/R_{ex}/R_I$ (%): 5.4/7.3/3.6/5.8

Atom	*x/a*	*y/b*	*z/c*	*B* (iso)	population/uc
Si	–.0543(2)	.0364(2)	.1256(2)	0.8	192
O1	–.1066(3)	0	.1066(3)	2.5	96
O2	–.0033(3)	–.0033(3)	.1428(5)	2.5	96
O3	–.0327(5)	.0759(3)	.0759(3)	2.5	96
O4	–.0722(4)	.0716(3)	.1784(3)	2.5	96
NaI	0	0	0	3.3	3(1)
NaI’	.0621(5)				26(1)
NaII	.2413(6)				27(1)
C1	.258	.338	.298	9.0	19(1)
H1	.227	.369	.298	9.0	
C2	.477	.477	.546	9.0	10(1)
H2	.459	.459	.582	9.0	
OW1	.167	.167	.171	9.0	3(1)
H11	.181	.134	.191	9.0	
H21	.134	.181	.191	9.0	
OW2	.211	.326	.326	9.0	15(1)
H21	.171	.331	.323	9.0	
H22	.221	.337	.366	9.0	

Si–O1 1.641(3) Si–O2 1.651(3) Si–O3 1.654(3) Si–O4 1.629(3)

Benzene coordinates, total Na/uc and thermal parameters fixed (see [4]). Water coordinates fixed according to MM simulations.

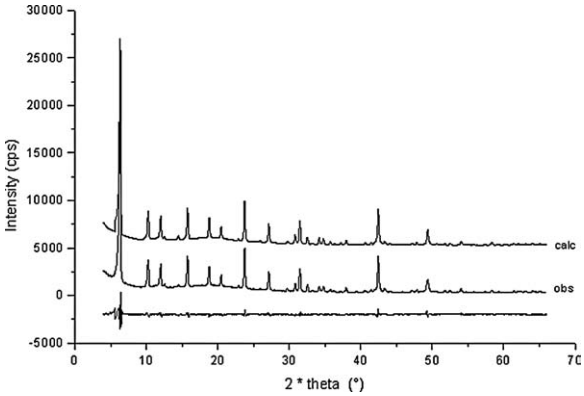

Fig. A.III.3. Rietveld plots for $Na_{56}Al_{56}Si_{136}O_{384}$·***29*** C_6H_6 + ***18*** H_2O (point 13 in Fig. 1).

Point 14

Sample label: PL52_BZ40

Sample formula: $Na_{56}Al_{56}Si_{136}O_{384}$·43 C_6H_6 + 18 H_2O

Sample origin: LZY-52 (Sigma–Aldrich)

Diffractometer: Philips – X′Pert – in air-tight brass sample-holder

Wavelength (Å): Cu Kα

Angular range (°2θ): 4–66

Angular step (°2θ): 0.025

Unit-cell parameter (Å): 24.690(1)

Number of observables: 2481 + 16 = 2497

Number of *hkl* triplets: 165

$R_p/R_{wp}/R_{ex}/R_I$ (%): 6.0/8.4/3.4/6.5

Atom	*x/a*	*y/b*	*z/c*	*B* (iso)	population/uc
Si	–.0543(2)	.0367(2)	.1264(2)	0.8	192
O1	–.1070(3)	0	.1070(3)	2.5	96
O2	–.0026(3)	–.0026(3)	.1416(5)	2.5	96
O3	–.0347(5)	.0762(3)	.0762(3)	2.5	96
O4	–.0732(4)	.0726(3)	.1774(3)	2.5	96
NaI	0	0	0	3.3	1(1)
NaI’	.0592(5)				25(1)
NaII	.2381(5)				30(1)
C1	.258	.338	.298	9.0	30(1)
H1	.227	.369	.298	9.0	
C2	.477	.477	.546	9.0	13(1)
H2	.459	.459	.582	9.0	
OW1	.167	.167	.171	9.0	8(1)
H11	.181	.134	.191	9.0	
H21	.134	.181	.191	9.0	
OW2	.211	.326	.326	9.0	10(1)
H21	.171	.331	.323	9.0	
H22	.221	.337	.366	9.0	

Si–O1 1.654(3) Si–O2 1.647(3) Si–O3 1.649(3) Si–O4 1.610(3).

Benzene coordinates, total Na/uc and thermal parameters fixed (see [4]). Water coordinates fixed according to MM simulations.

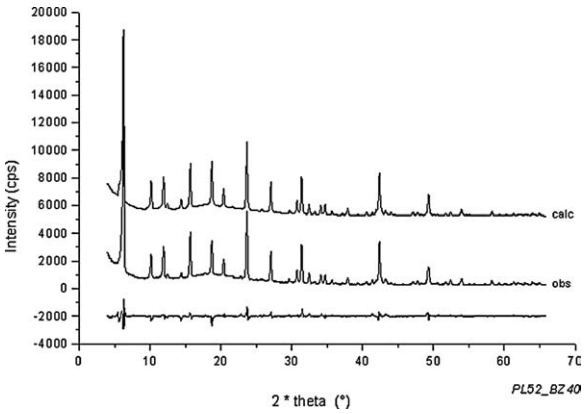

Fig. A.III.4. Rietveld plots for $Na_{56}Al_{56}Si_{136}O_{384}$·***43*** C_6H_6 + ***18*** H_2O (point 14 in Fig. 1).

References

[1] W.M. Meier, D.H. Olson, Atlas of Zeolite Structure Types, Butterworths, London, 1987.
[2] D.W. Breck, Zeolite Molecular Sieves, Wiley, New York, 1974.
[3] R.M. Barrer, Zeolites and Clay Minerals as Sorbents and Molecular Sieves, Academic Press, London, 1978.
[4] A.N. Fitch, H. Jobic, A. Renouprez, J. Phys. Chem. 90 (1986) 1311 [NaY(56)].
[5] S. Buttefey, A. Boutin, C. Mellot-Draznieks, A.H. Fuchs, J. Phys. Chem. B 105 (2001) 9569.
[6] B.-H. Ha, D. Barthomeuf, Y. Trambouze, J. Chim. Phys. 3 (1973) 463.
[7] D. Barthomeuf, B.-H. Ha, J. Chem. Soc., Farad. Trans I 69 (1973) 2147.
[8] D. Barthomeuf, B.-H. Ha, J. Chem. Soc., Farad. Trans I 69 (1973) 2158.
[9] A. de Mallmann, D. Barthomeuf, in: 7h IZC, Tokyo, 1986, p. 609 (AD-8-1).
[10] W. Schirmer, H. Thamm, H. Stach, U. Lohse, The Properties and Applications of Zeolites, J. Chem. Soc. (Lond.) Spec. Publ. 33 (1979) 204.
[11] B.-L. Su, B. Norberg, Colloids and Surfaces, A, Physicochem. Eng. Aspects 187–188 (2001) 297.
[12] B.-L. Su, V. Norberg, J.A. Martens, Langmuir 17 (2001) 1267.
[13] Y.-H. Chen, L.-P. Hwang, Magn. Reson. Chem. 37 (1999) S84.
[14] A. de Mallmann, D. Barthomeuf, Zeolites 8 (1988) 292.
[15] C. Pichon, A. Méthivier, M.-H. Simonot-Grange, C. Baerlocher, J. Phys. Chem. B 103 (1999) 10197.
[16] G. Vitale, C.F. Mellot, L.M. Bull, A.K. Cheetham, J. Phys. Chem. B 101 (1997) 4559.
[17] Y.H. Yeom, A.N. Kim, Y. Kim, S.H. Song, K. Seff, J. Phys. Chem. B 102 (1998) 6071.
[18] G. Vitale, L.M. Bull, R.E. Morris, A.K. Cheetham, B.H. Toby, C.G. Coe, J.E. MacDougall, J. Phys. Chem. 99 (1995) 16087.
[19] B. Geil, O. Isfort, B. Boddenberg, D.E. Favre, B.F. Chmelka, F. Fujara, J. Chem. Phys. 116 (2002) 2184.
[20] H. Stach, U. Lohse, H. Thamm, W. Schirmer, Zeolites 6 (1986) 74.
[21] B.F. Mentzen, F. Di Renzo, C.R. Acad. Sci., Ser. II 321 (1995) 343.
[22] J.A. Hriljac, M.M. Eddy, A.K. Cheetham, J.A. Donohue, J. Ray, J. Solid-State Chem. 106 (1993) 66.
[23] K. Bobuatong, J. Limtrakul, Appl. Catal. A 253 (2003) 49.
[24] S. Kasuriya, S. Namuangruk, P. Treesukol, M. Tirtowidjojo, J. Limtrakul, J. Catal. 219 (2003) 320.
[25] S. Kasuriya, S. Namuangruk, P. Treesukol, M. Tirtowidjojo, J. Limtrakul, J. Catal. 219 (2003) 320.
[26] L. Uytterhoeven, D. Dompas, W.J. Mortier, J. Chem. Soc., Farad. Trans. 88 (1992) 2753.
[27] S.M. Auerbach, N.J. Henson, A.K. Cheetham, H.I. Metiu, J. Phys. Chem. 99 (1995) 10600.
[28] B.F. Mentzen, F. Bosselet, J. Bouix, C.R. Acad. Sci., Ser. II 306 (1988) 27.
[29] B.F. Mentzen, F. Lefebvre, Mater. Res. Bull. 30 (1995) 613.
[30] B.F. Mentzen, Mater. Res. Bull. 30 (1995) 1193.
[31] D.E. Williams, Acta Crystallogr. A 36 (1980) 715.
[32] D.B. Wiles, R.A. Young, J. Appl. Crystallogr. 14 (1981) 149 and a locally modified version of the DBW-32 code.
[33] A.C. Larson, R.B. Von Dreele, in: General Structure Analysis System (GSAS), Los Alamos National Laboratory Report LAUR, 1994, p. 86.
[34] G.E. Bacon, N.A. Curry, S.A. Wilson, Proc. R. Soc, Lond., Ser. A 279 (1964) 98.